JOURNAL FOR SOCIAL SCIENCE STUDIES
An International Peer-Reviewed Open Access Journal

ISSN (Online): 3006-2071 | ISSN (Print): 3006-2063
Volume 4 • Issue 4 • August 2026

NUMERICAL ANALYSIS OF NON-NEWTONIAN NANOFLUID FLOW WITH THERMAL RADIATION AND HEAT GENERATION

Abdul Razaq[1], Shawal Rizwan*[2], Zahid Nawaz[3], Hamza Khan*[4], Rabail Urooj[5], Kiramat Ullah[6]

[1]*COMSATS University Islamabad, Pakistan.*
[*2] *Department of Mathematics, Islamia College University, Peshawar, KPK, Pakistan.*
[3]*Department of Mathematics, Northern University Nowshera, KPK, Pakistan*
[4]*Bachelor in Physics, University of Swat, KPK, Pakistan*
[5]*Assistant Professor, Department of Environmental Sciences, Sardar Bahadur Khan Women's University, Quetta, Pakistan*
[6] *Department of Numerical Science, Kohat University of Science & Technology, Kohat – 26000, KPK, Pakistan*

[*2]shawalrizwan71@gmail.com , [*4]hamzakhannji0987@gmail.com

DOI: https://doi.org/10.5281/zenodo.22668348

Keywords
Al_2O_3–water nanofluid, thermal radiation, internal heat generation, boundary-layer flow, numerical analysis.

Article History
Received: 28 June 2026
Accepted: 15 August 2026
Published: 31 August 2026

Copyright @Author
Corresponding Author: *
Shawal Rizwan

Abstract

This study presents a numerical investigation of steady Casson Al_2O_3–water nanofluid flow over a linearly stretching sheet under the combined effects of thermal radiation and uniform internal heat generation. The governing boundary-layer equations were transformed into a nonlinear system of ordinary differential equations and solved using a collocation-based boundary-value method. The effects of the Casson parameter, nanoparticle volume fraction, radiation parameter, and heat-generation parameter on wall shear and thermal transport were systematically examined. The results show that increasing the Casson parameter from 0.5 to 10 decreases the dimensionless skin-friction response from 1.7388 to 1.0527, indicating a gradual transition toward Newtonian behavior. Increasing the radiation parameter from 0 to 2 reduces the dimensionless wall-temperature gradient from 1.5967 to 0.8445 because of enhanced effective thermal diffusion. Increasing the Al_2O_3 volume fraction from 0 to 0.04 decreases the wall-temperature gradient while increasing the conductivity-weighted heat-transfer measure from 1.3173 to 1.3728. Internal heat generation increases the thermal energy within the boundary layer and reduces the wall-temperature gradient, while producing essentially no change in the hydrodynamic response. For the reference case, with a Casson parameter of 1, nanoparticle volume fraction of 0.02, radiation parameter of 0.5, and heat-generation parameter of 0.1, the dimensionless skin-friction response is approximately 1.4195 and the wall-temperature gradient is 1.2707, with a conductive heat-transfer measure of approximately 1.3450. The recovery of the Newtonian limiting behavior further confirms the consistency of the numerical formulation. The findings demonstrate that rheological, nanoparticle, radiative, and thermal-generation effects should be considered collectively in the design of non-Newtonian nanofluid thermal-processing and heat-transfer systems.

JOURNAL FOR SOCIAL SCIENCE STUDIES
An International Peer-Reviewed Open Access Journal
ISSN (Online): 3006-2071 | ISSN (Print): 3006-2063
Volume 4 • Issue 4 • August 2026

1. Introduction

Nanofluids are engineered suspensions of nanoscale solid particles dispersed in conventional heat-transfer fluids, such as water, ethylene glycol, and other base liquids. Their development has attracted considerable attention because the incorporation of nanoparticles can substantially modify the effective thermal conductivity, viscosity, heat capacity, and overall thermal transport characteristics of the base fluid. These enhanced properties make nanofluids promising for applications involving thermal management and energy transport, including electronic cooling, heat exchangers, thermal processing, energy conversion systems, cooling of manufacturing equipment, and advanced heat-transfer devices. The nanofluid concept introduced by Choi and Eastman provided an important foundation for improving the thermal transport capability of conventional fluids through the addition of nanoscale particles [1]. Subsequent investigations have focused on both effective-property models and more detailed descriptions of nanoparticle transport. In particular, Buongiorno identified Brownian diffusion and thermophoresis as important mechanisms when nanoparticle–fluid relative motion is explicitly considered [2]. The selection of an appropriate nanofluid model therefore depends strongly on the physical characteristics of the flow configuration and the mechanisms that are intended to be investigated.

In many practical processing and engineering systems, the working fluids do not exhibit purely Newtonian behavior [4]. Non-Newtonian fluids are characterized by a nonlinear relationship between shear stress and shear rate and may exhibit shear-dependent viscosity, yield stress, or other rheological characteristics. Such behavior is encountered in polymer solutions, concentrated suspensions, paints, drilling fluids, biological materials, food-processing fluids, and molten process materials. For these applications, the use of a Newtonian assumption may not adequately represent the underlying momentum transport. The Casson model provides a relatively simple and useful constitutive description for fluids possessing yield-stress characteristics and has consequently been employed in numerous studies of boundary-layer flow, stretching surfaces, extrusion, coating processes, and biomedical transport [5, 6]. An important feature of the Casson formulation is the Casson parameter, β, which provides a convenient measure of the fluid's departure from Newtonian behavior. As β increases, the Casson fluid progressively approaches the Newtonian limiting condition, allowing the influence of non-Newtonian rheology to be assessed within a unified mathematical framework. The flow of a fluid over a stretching sheet represents a classical boundary-layer problem with significant relevance to industrial manufacturing and material-processing operations. During polymer extrusion, continuous casting, wire coating, glass-fiber production, plastic-film manufacturing, and related processes, a continuously moving or stretching surface induces fluid motion and simultaneously affects the development of the thermal boundary layer. The interaction between surface stretching, fluid rheology, and heat transfer can therefore have a direct influence on product quality, surface shear, cooling rate, and thermal uniformity. The stretching-sheet configuration also provides a mathematically tractable framework in which the effects of different physical parameters can be systematically investigated. Consequently, this formulation has been extensively extended to nanofluids and non-Newtonian fluids by incorporating additional thermal and transport mechanisms [6,7].

Thermal radiation represents another important heat-transfer mechanism, particularly in systems operating at relatively high temperatures [8]. When radiative heat transfer becomes significant compared with conductive heat transfer, neglecting radiation may lead to an incomplete description of the thermal field. For an optically thick medium, the Rosseland diffusion approximation offers a practical approach for representing radiative heat flux and allows radiation to be incorporated into the energy equation through an effective

JOURNAL FOR SOCIAL SCIENCE STUDIES
An International Peer-Reviewed Open Access Journal
ISSN (Online): 3006-2071 | ISSN (Print): 3006-2063
Volume 4 • Issue 4 • August 2026

thermal-diffusion contribution. Previous investigations have examined the combined effects of radiation and Casson nanofluid flow, often together with magnetic fields, porous media, chemical reactions, surface slip, suction or injection, Brownian motion, thermophoresis, and internal heat generation [9]. Although such multiphysics models can provide valuable information for specialized applications, simultaneously incorporating numerous mechanisms increases mathematical complexity and can make it difficult to isolate the individual contribution of the principal rheological and thermal parameters. Internal heat generation is also relevant to thermal systems in which energy is produced within the fluid volume rather than supplied exclusively through the boundaries. Volumetric heat generation can alter the temperature distribution, thermal boundary-layer thickness, and heat-transfer rate at the stretching surface. Its interaction with thermal radiation is particularly important because both mechanisms directly influence the energy balance. A systematic assessment of these effects is therefore useful for understanding the thermal response of non-Newtonian nanofluids under controlled operating conditions [10]. At the same time, increasing the number of physical effects in a mathematical model does not necessarily improve its ability to explain individual mechanisms. A reduced formulation can be advantageous when the primary objective is to establish clear parameter–response relationships.

Accordingly, the present study considers a deliberately reduced but physically meaningful model of steady Casson Al_2O_3–water nanofluid flow over a linearly stretching sheet. Thermal radiation is incorporated using the Rosseland approximation, while uniform volumetric heat generation is retained in the energy equation [11]. In order to maintain a controlled framework, magnetic-field effects, porous-medium resistance, chemical reaction, velocity slip, suction/injection, Brownian diffusion, thermophoresis, and viscous dissipation are excluded. This formulation allows the effects of the Casson parameter (β), nanoparticle volume fraction (φ), radiation parameter (R_d), and heat-generation parameter (Q) to be examined independently and in combination. Particular attention is given to their influence on the velocity and temperature profiles and on the engineering quantities associated with surface friction and heat transfer. The principal objectives of the study are therefore to: (i) formulate a consistent mathematical model for steady Casson Al_2O_3–water nanofluid flow over a linearly stretching sheet; (ii) incorporate thermal radiation through the Rosseland diffusion approximation; (iii) account for uniform internal heat generation within the thermal boundary layer; (iv) numerically quantify the effects of β, φ, R_d, and Q on velocity, temperature, skin-friction, and heat-transfer characteristics; and (v) verify the formulation by examining the Newtonian limiting behavior as β tends to infinity. The resulting framework is intended to provide a focused numerical assessment of the coupled rheological and thermal effects rather than a comprehensive multiphysics representation. By restricting the model to the dominant mechanisms considered here, the study provides a clearer physical interpretation of how non-Newtonian behavior, nanoparticle loading, thermal radiation, and internal heat generation govern the transport characteristics of Casson nanofluid flow over a stretching surface.

2. Methodology

2.1 Physical model and assumptions

A steady, incompressible, two-dimensional Casson nanofluid flow is considered over a flat stretching sheet located at. The x-axis is taken along the sheet and the y-axis normal to it. The sheet stretches linearly with velocity. The physical configuration and development of the hydrodynamic and thermal boundary layers are illustrated in Figure 1.

JOURNAL FOR SOCIAL SCIENCE STUDIES
An International Peer-Reviewed Open Access Journal
ISSN (Online): 3006-2071 | ISSN (Print): 3006-2063
Volume 4 • Issue 4 • August 2026

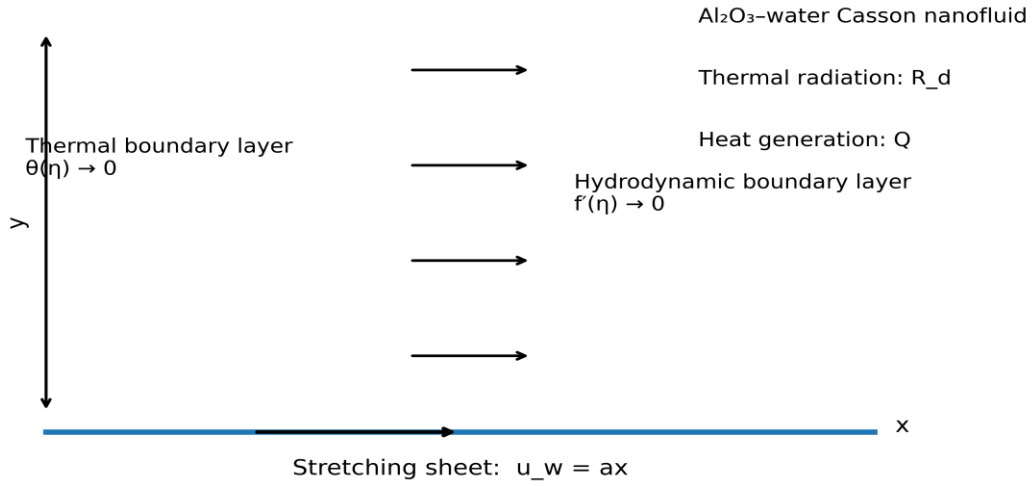


Figure 1. Physical configuration of the Casson Al_2O_3–water nanofluid flow over a linearly stretching sheet.

$$u_w = ax,\ a > 0,$$

where a is the stretching rate. The wall and ambient temperatures are denoted by T_w and T_∞, respectively, with $T_w > T_\infty$. The flow is analyzed under the steady boundary-layer approximation with negligible pressure-gradient effects and constant effective thermophysical properties for a given nanoparticle volume fraction. The Al_2O_3–water nanofluid is treated as a single-phase fluid. Viscous dissipation, magnetic-field effects, porous-medium resistance, chemical reaction, velocity slip, suction/injection, Brownian motion, and thermophoresis are neglected. Thermal radiation is considered using the Rosseland approximation for an optically thick medium, while uniform volumetric heat generation is included in the energy equation. These assumptions allow the effects of the Casson parameter β, nanoparticle volume fraction ϕ, radiation parameter R_d, and heat-generation parameter Q to be investigated systematically.

2.2 Effective thermophysical properties

The Al_2O_3–water nanofluid is modeled using the conventional single-phase effective-property approach, in which the suspended nanoparticles and base fluid are treated as a homogeneous mixture [12]. The nanoparticle volume fraction, denoted by ϕ, determines the contribution of Al_2O_3 particles to the effective thermophysical properties of the nanofluid. The effective density is obtained from the volumetric mixing relation, while the effective volumetric heat capacity represents the combined ability of the base fluid and nanoparticles to store thermal energy. These properties are expressed as

$$\rho_{nf} = (1-\phi)\rho_f + \phi\rho_s \qquad (1)$$

and

$$(\rho C_p)_{nf} = (1-\phi)(\rho C_p)_f + \phi(\rho C_p)_s. \qquad (2)$$

Here, the subscripts nf, f, and s represent the nanofluid, base fluid, and solid nanoparticles, respectively. Equation (1) shows that increasing the nanoparticle concentration increases the effective density because Al_2O_3 has a considerably higher density than water. Similarly, Equation (2) accounts for the combined volumetric heat-storage capacity of the two phases and is used in determining the thermal response of the nanofluid.

The effective dynamic viscosity is evaluated using the Brinkman model, which accounts for the increase in flow resistance associated with the addition of solid nanoparticles:

JOURNAL FOR SOCIAL SCIENCE STUDIES
An International Peer-Reviewed Open Access Journal
ISSN (Online): 3006-2071 | ISSN (Print): 3006-2063
Volume 4 • Issue 4 • August 2026

$$\mu_{nf} = \frac{\mu_f}{(1-\phi)^{2.5}}. \quad (3)$$

The corresponding kinematic viscosity and thermal diffusivity are then calculated from

$$\nu_{nf} = \frac{\mu_{nf}}{\rho_{nf}}, \quad (4)$$

$$\alpha_{nf} = \frac{k_{nf}}{(\rho C_p)_{nf}}. \quad (5)$$

The effective thermal conductivity is determined using the Maxwell model, which is appropriate for a dilute suspension of solid particles in a continuous fluid medium:

$$k_{nf} = k_f \left[\frac{k_s + 2k_f - 2\phi(k_f - k_s)}{k_s + 2k_f + \phi(k_f - k_s)}\right]. \quad (6)$$

Because Al_2O_3 possesses substantially higher thermal conductivity than water, increasing ϕ generally enhances the effective thermal conductivity of the nanofluid. The thermophysical properties of water and Al_2O_3 used in the present numerical calculations are summarized in **Table 1**. These effective-property relations distinguish the nanofluid properties from those of the base fluid and provide the material-property basis for the subsequent momentum and energy equations [3,11–13].

Table 1. Thermophysical properties used in the numerical model.

Property	Water	Al_2O_3
Density, ρ (kg m^{-3})	997.1	3970
Specific heat, C_p (J kg^{-1} K^{-1})	4179	765
Thermal conductivity, k (W m^{-1} K^{-1})	0.613	40
Dynamic viscosity, μ (Pa s)	8.90 × 10^{-4}	–

2.3 Casson rheological model

For the boundary-layer formulation, Casson rheology enters through the factor (1 + 1/β), where β is the dimensionless Casson parameter. Lower β values represent stronger non-Newtonian effects, whereas β → ∞ corresponds to Newtonian behavior. The effective momentum-diffusion coefficient is therefore

$$\nu_{nf}(1 + 1/\beta) \quad (7)$$

and the Newtonian limiting relation is

$$(1 + 1/\beta) \to 1 \ \text{as} \ \beta \to \infty \quad (8)$$

2.4 Governing equations

Under the stated assumptions, the continuity equation is

$$\partial u/\partial x + \partial v/\partial y = 0 \quad (9)$$

The Casson momentum equation is

$$u(\partial u/\partial x) + v(\partial u/\partial y) = \nu_{nf}(1 + 1/\beta)(\partial^2 u/\partial y^2) \quad (10)$$

The energy equation, including thermal radiation and uniform heat generation, is

$$u(\partial T/\partial x) + v(\partial T/\partial y) = \alpha_{nf}(\partial^2 T/\partial y^2) - [1/(\rho C_p)_{nf}](\partial q_r/\partial y) + [Q_0/(\rho C_p)_{nf}](T - T_\infty) \quad (11)$$

2.5 Thermal radiation model

The Rosseland approximation is used for the radiative heat flux:

$$q_r = -(4\sigma^*/3k^*)\,\partial(T^4)/\partial y \quad (12)$$

For relatively small temperature differences, T^4 is linearized about T_∞ according to

$$T^4 \approx 4T_\infty^3 T - 3T_\infty^4 \quad (13)$$

$$\partial(T^4)/\partial y \approx 4T_\infty^3(\partial T/\partial y) \quad (14)$$

$$q_r = -[16\sigma^* T_\infty^3/(3k^*)](\partial T/\partial y) \quad (15)$$

$$-\partial q_r/\partial y = [16\sigma^* T_\infty^3/(3k^*)](\partial^2 T/\partial y^2) \quad (16)$$

Accordingly, radiation acts as an additional contribution to thermal diffusion. The dimensionless radiation parameter is defined as

JOURNAL FOR SOCIAL SCIENCE STUDIES
An International Peer-Reviewed Open Access Journal
ISSN (Online): 3006-2071 | ISSN (Print): 3006-2063
Volume 4 • Issue 4 • August 2026

$$R_d = 16\sigma^* T_\infty^3/(3k^* k_{nf}) \quad (17)$$

2.6 Similarity transformation

To transform the governing partial differential equations into a system of nonlinear ordinary differential equations, a suitable similarity transformation is introduced. The similarity variable ηcombines the spatial coordinates and the stretching rate and represents the dimensionless distance measured normal to the stretching surface. It is defined as

$$\eta = y\sqrt{\frac{a}{\nu_f}}. \quad (18)$$

A stream function is introduced to automatically satisfy the continuity equation. The corresponding stream function is written as

JOURNAL FOR SOCIAL SCIENCE STUDIES
An International Peer-Reviewed Open Access Journal
ISSN (Online): 3006-2071 | ISSN (Print): 3006-2063
Volume 4 • Issue 4 • August 2026

$$\psi = x\sqrt{a\nu_f}\, f(\eta), \qquad (19)$$

where $f(\eta)$is the dimensionless similarity function and $\nu_f$denotes the kinematic viscosity of the base fluid. Using the standard definitions $u = \partial\psi/\partial y$and $v = -\partial\psi/\partial x$, the velocity components in the x- and y-directions are obtained as

$$u = axf'(\eta),\ v = -\sqrt{a\nu_f}\, f(\eta). \qquad (20)$$

Thus, the dimensional velocity field is represented in terms of a single similarity function, with $f'(\eta)$describing the dimensionless streamwise velocity distribution and $f(\eta)$governing the normal velocity component.

The temperature field is nondimensionalized using the wall-to-ambient temperature difference. The dimensionless temperature is defined as

$$\theta(\eta) = \frac{T - T_\infty}{T_w - T_\infty}. \qquad (21)$$

Accordingly, the dimensional temperature can be recovered from

$$T = T_\infty + (T_w - T_\infty)\theta(\eta). \qquad (22)$$

With this transformation, $\theta = 1$at the stretching surface and $\theta \to 0$far from the surface. The above similarity transformations reduce the governing momentum and energy equations from partial differential equations to coupled nonlinear ordinary differential equations in the single independent variable η, thereby providing a convenient formulation for the subsequent numerical solution.

2.7 Reduced ordinary differential equations

Upon substituting the similarity transformations given in Eqs. (18)–(22) into the governing momentum and energy equations, the original partial differential equations are reduced to a coupled system of nonlinear ordinary differential equations in terms of the similarity variable η. The transformed momentum equation describing the dimensionless velocity field is

$$A_m f''' + ff'' - (f')^2 = 0. \qquad (23)$$

Here, f, f', and f''represent the dimensionless stream function and its derivatives with respect to η. The parameter $A_m$incorporates the effects of nanofluid viscosity, density, and Casson rheology and is defined as

$$A_m = \left(\frac{\nu_{nf}}{\nu_f}\right)\left(1 + \frac{1}{\beta}\right). \qquad (24)$$

Thus, variations in the Casson parameter βdirectly influence the momentum transport. In the limiting case of $\beta \to \infty$, the Casson contribution approaches unity and the model recovers the corresponding Newtonian behavior. The transformed energy equation, including thermal radiation and uniform internal heat generation, is expressed as

$$A_T\theta'' + f\theta' + Q\theta = 0. \qquad (25)$$

The effective thermal parameter $A_T$is given by

$$A_T = \left(\frac{\alpha_{nf}}{\nu_f}\right)(1 + R_d), \qquad (26)$$

JOURNAL FOR SOCIAL SCIENCE STUDIES
An International Peer-Reviewed Open Access Journal
ISSN (Online): 3006-2071 | ISSN (Print): 3006-2063
Volume 4 • Issue 4 • August 2026

where α_{nf} is the thermal diffusivity of the nanofluid and R_d is the dimensionless radiation parameter. The factor $(1 + R_d)$ represents the additional contribution of thermal radiation to the effective thermal diffusion within the boundary layer. The heat-generation parameter is defined as

$$Q = \frac{Q_0}{a(\rho C_p)_{nf}}, \qquad (27)$$

where Q_0 denotes the uniform volumetric heat-generation coefficient. A larger value of Q represents stronger internal heat production and consequently modifies the temperature distribution within the fluid. Therefore, R_d measures the relative contribution of radiative thermal diffusion, whereas Q characterizes the strength of internal heating relative to the characteristic stretching-flow timescale. Together, Eqs. (23)–(27) provide the dimensionless formulation used for the subsequent numerical analysis.

2.8 Boundary conditions

The boundary conditions are specified at the stretching surface and in the far-field region. At the sheet surface ($\eta = 0$), the fluid satisfies the no-penetration condition, the streamwise fluid velocity is equal to the stretching velocity of the sheet, and the fluid temperature is maintained at the wall temperature T_w. These conditions are expressed as

$$f(0) = 0,\ f'(0) = 1,\ \theta(0) = 1. \qquad (28)$$

Here, $f(0) = 0$ represents zero normal velocity at the impermeable stretching surface, $f'(0) = 1$ ensures that the fluid moves with the prescribed stretching velocity, and $\theta(0) = 1$ corresponds to $T = T_w$ at the wall.

Far away from the stretching surface, the influence of the sheet diminishes and the fluid approaches the quiescent ambient state. Therefore, the dimensionless velocity and temperature satisfy

$$f'(\infty) = 0,\ \theta(\infty) = 0. \qquad (29)$$

Thus, the velocity approaches zero relative to the stationary ambient fluid, while the temperature approaches the ambient temperature T_∞. In the numerical calculations, the infinite computational domain is approximated by a sufficiently large finite value of the similarity variable.

2.9 Engineering quantities

The local Reynolds number is

$$Re_x = u_w\, x/\nu_f = a x^2/\nu_f \quad (30)$$

The local skin-friction coefficient is

$$C_f = 2\tau_w/(\rho_{nf}\, u_w^2) \quad (31)$$

$$\tau_w = \mu_{nf}(1 + 1/\beta)(\partial u/\partial y)|_{y=0} \quad (32)$$

$$C_f\, Re_x^{1/2} = -2A_m\, f''(0) \quad (33)$$

Because the manuscript tables report the conductivity-weighted conductive heat-transfer response rather than the total heat flux including radiation, the tabulated quantity is defined as

$$Nu_x\, Re_x^{-1/2}\,|_{conductive} = (k_{nf}/k_f)[-\theta'(0)] \quad (34)$$

If both conduction and Rosseland radiation are included in the wall heat flux, the corresponding total heat-transfer measure is

$$Nu_x\, Re_x^{-1/2}\,|_{total} = (k_{nf}/k_f)(1 + R_d)[-\theta'(0)] \quad (35)$$

This distinction corrects an ambiguity in the source material: the numerical values in Tables 2–5 correspond to the conductivity-weighted conductive measure, whereas Eq. (35) is the total wall heat-transfer measure when radiative heat flux is explicitly included.

JOURNAL FOR SOCIAL SCIENCE STUDIES
An International Peer-Reviewed Open Access Journal
ISSN (Online): 3006-2071 | ISSN (Print): 3006-2063
Volume 4 • Issue 4 • August 2026

2.10 Numerical solution procedure

The third-order momentum equation and second-order energy equation are converted into five first-order equations by defining $y_1 = f$, $y_2 = f'$, $y_3 = f''$, $y_4 = \theta$, and $y_5 = \theta'$. The resulting system is

$$y_1' = y_2 \quad (36)$$
$$y_2' = y_3 \quad (37)$$
$$y_3' = [(y_2)^2 - y_1 y_3]/A_m \quad (38)$$
$$y_4' = y_5 \quad (39)$$
$$y_5' = -(y_1 y_5 + Q y_4)/A_T \quad (40)$$

The semi-infinite computational domain is truncated at $\eta_{max} = 12$, for which the far-field conditions are approximated by $f'(12) \approx 0$ and $\theta(12) \approx 0$. A collocation-based boundary-value algorithm is used with a convergence tolerance of 10^{-7}. Mesh refinement is continued until the wall-gradient quantities remain unchanged to the reported precision. The representative reference case is $\beta = 1$, $\varphi = 0.02$, $R_d = 0.5$, and $Q = 0.1$.

3. Results and Discussion

The numerical results quantify the effects of the four principal control parameters—Casson parameter β, radiation parameter R_d, heat-generation parameter Q, and nanoparticle volume fraction φ—on wall shear and thermal transport. Unless otherwise stated, the reference case is $\beta = 1$, $\varphi = 0.02$, $R_d = 0.5$, and $Q = 0.1$. For this reference state, the predicted dimensionless skin-friction response is $C_f Re_x^{1/2} \approx 1.4195$ and the wall-temperature gradient is $-\theta'(0) = 1.2707$.

3.1 Effect of the Casson parameter

The Casson parameter, β, is an important rheological parameter that characterizes the degree of non-Newtonian behavior of the fluid. In the present formulation, lower values of β represent stronger Casson effects, whereas increasing β progressively weakens the non-Newtonian contribution, approaching the Newtonian limit. The corresponding effects on the wall velocity gradient, temperature gradient, skin-friction coefficient, and heat-transfer rate are summarized in Table 2.

As shown in Table 2, increasing β from 0.5 to 10 causes $-f''(0)$ to increase substantially from 0.5796 to 0.9570. At the same time, the dimensionless skin-friction coefficient $C_f Re_x^{1/2}$ decreases from 1.7388 to 1.0527. This behavior indicates that the Casson rheology has a strong influence on the momentum boundary layer. At small β the non-Newtonian character of the fluid is more pronounced, producing a larger rheological correction in the momentum equation. As β increases, this correction becomes progressively weaker, and the flow approaches Newtonian behavior. This interpretation is consistent with previous numerical investigations of Casson fluids and Casson nanofluids over stretching surfaces, which have demonstrated that variations in the Casson parameter significantly modify the velocity field and wall-shear characteristics [13,14].

The results in Table 2 further show that the limiting value of $-f''(0)$ approaches unity, reaching approximately 1.0037 in the Newtonian limit. This convergence provides an important consistency check for the present mathematical formulation because the Casson model should recover Newtonian behavior as $\beta \to \infty$. The corresponding reduction in $C_f Re_x^{1/2}$ from 1.7388 at $\beta = 0.5$ to approximately 1.0037 in the Newtonian limit indicates that the wall-shear response is strongest when the Casson effects are most pronounced. A comparatively moderate influence is observed on the thermal characteristics. According to Table 2, the wall-temperature gradient $-\theta'(0)$ decreases from 1.3037 at $\beta = 0.5$ to 1.1943 in the Newtonian limit. Similarly, the conductivity-weighted heat-transfer measure, $Nu_x Re_x^{-1/2}$, decreases from 1.3799 to 1.2641. Thus, increasing β produces a gradual reduction in the predicted heat-transfer rate. The weaker thermal response compared with the hydrodynamic response

JOURNAL FOR SOCIAL SCIENCE STUDIES
An International Peer-Reviewed Open Access Journal
ISSN (Online): 3006-2071 | ISSN (Print): 3006-2063
Volume 4 • Issue 4 • August 2026

suggests that, under the present parameter settings, Casson rheology primarily controls the momentum field, while its influence on the thermal boundary layer occurs through coupling with the velocity field. A similar dependence of heat-transfer characteristics on the Casson parameter has been reported for radiative Casson nanofluid flow over stretching surfaces [15,16].

Overall, the results presented in Table 2 demonstrate that increasing the Casson parameter causes the fluid to transition from strongly non-Newtonian Casson behavior toward the Newtonian state. The most pronounced changes occur in the wall velocity gradient and skin-friction response, whereas the wall-temperature gradient and conductive heat-transfer rate exhibit comparatively smaller but systematic reductions. These findings confirm that the Casson parameter is an important control parameter for regulating both momentum transport and, through hydrodynamic–thermal coupling, heat transfer in non-Newtonian nanofluid flow over a stretching surface. The corresponding variation of the dimensionless wall-shear measure with β is shown in Figure 2.

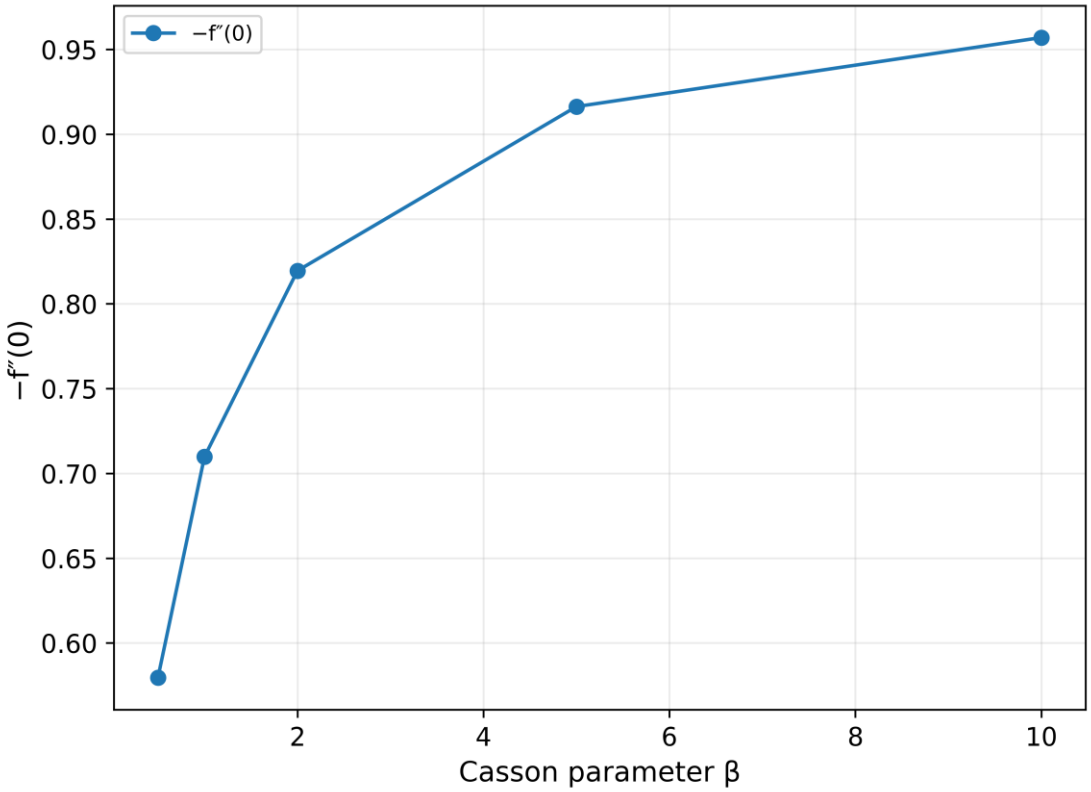


Figure 2. Variation of the dimensionless wall-shear measure, −f″(0), with the Casson parameter β.

Table 2. Effect of the Casson parameter on flow and heat-transfer characteristics.

β	−f″(0)	−θ′(0)	C_f Re_x^1/2	Conductive Nu_x Re_x^−1/2
0.5	0.5796	1.3037	1.7388	1.3799
1.0	0.7098	1.2707	1.4195	1.3450
2.0	0.8195	1.2425	1.2293	1.3151
5.0	0.9163	1.2173	1.0995	1.2885
10.0	0.9570	1.2066	1.0527	1.2772
∞ (Newtonian	≈1.0037	1.1943	≈1.0037	1.2641

JOURNAL FOR SOCIAL SCIENCE STUDIES
An International Peer-Reviewed Open Access Journal
ISSN (Online): 3006-2071 | ISSN (Print): 3006-2063
Volume 4 • Issue 4 • August 2026

limit)				

2 Velocity profile

The dimensionless velocity distribution is represented by (f'(\eta)), where (\eta) denotes the similarity variable normal to the stretching surface. At the wall, the boundary condition (f'(0)=1) satisfies the prescribed stretching velocity of the sheet, while (f'(\eta)\rightarrow0) as (\eta\rightarrow\infty), indicating that the fluid velocity gradually approaches the ambient condition away from the surface. The velocity boundary layer is primarily controlled by the competition between convective transport and the effective momentum diffusivity, which in the present Casson formulation is characterized by (\nu_{nf}(1+1/\beta)).

Variation of the Casson parameter therefore modifies the velocity-gradient distribution within the boundary layer. As indicated by the numerical values in Table 2, increasing (\beta) from 0.5 to 10 increases (-f''(0)) from 0.5796 to 0.9570, demonstrating a systematic change in the wall velocity gradient as the non-Newtonian contribution becomes weaker. At the same time, (C_fRe_x^{1/2}) decreases from 1.7388 to 1.0527 (Table 2), confirming that the Casson parameter has a pronounced effect on wall shear. For small (\beta), the stronger Casson character produces greater rheological modification of the momentum field, whereas increasing (\beta) progressively reduces this effect. As (\beta) becomes large, the Casson correction diminishes, and the velocity solution approaches the Newtonian limiting profile. This is also reflected in Table 2, where (-f''(0)) approaches approximately unity in the Newtonian limit. Such convergence is consistent with the fundamental behavior of the Casson model, for which the Newtonian fluid is recovered as the Casson parameter tends to infinity. Similar trends have been reported in studies of Casson and Casson nanofluid flow over stretching surfaces, where the Casson parameter was found to significantly influence the velocity field, wall velocity gradient, and skin-friction coefficient [17, 18]. Overall, the velocity behavior confirms that (\beta) is an important rheological control parameter. Its effect is particularly evident near the stretching surface, where changes in rheological resistance directly modify the velocity gradient and wall shear. The smooth approach toward the Newtonian solution with increasing (\beta) further supports the consistency of the present numerical formulation.

3.3 Effect of thermal radiation

Thermal radiation primarily modifies the thermal field and does not appear directly in the momentum equation. Consequently, the hydrodynamic quantities remain unchanged as the radiation parameter (R_d) varies. As evident from Table 3, (-f''(0)) remains constant at 0.7098, while (C_fRe_x^{1/2}) remains 1.4195 for all considered values of (R_d). This behavior confirms that, within the assumptions of the present model, thermal radiation does not directly alter the momentum boundary layer or wall shear stress. Similar behavior has been reported for radiative boundary-layer flows, where radiation primarily affects temperature distribution and heat transfer while the velocity field is governed by the momentum equation [19, 20]. In contrast, a pronounced effect is observed in the thermal characteristics. As shown in Table 3, increasing (R_d) from 0 to 2 causes the wall temperature gradient (-\theta'(0)) to decrease from 1.5967 to 0.8445. This reduction is associated with the increase in the effective thermal-diffusion coefficient (A_T), which contains the factor ((1+R_d)). Therefore, increasing thermal radiation enhances the effective diffusion of thermal energy within the boundary layer and reduces the magnitude of the wall temperature gradient. The progressive decrease from 1.5967 at (R_d=0) to 1.2707 at (R_d=0.5), 1.0760 at (R_d=1), and 0.8445 at (R_d=2) demonstrates that the thermal response is highly sensitive to the radiation parameter.

The same trend is reflected in the conductivity-weighted conductive heat-transfer measure. According to Table 3, (Nu_xRe_x^{-1/2})

JOURNAL FOR SOCIAL SCIENCE STUDIES
An International Peer-Reviewed Open Access Journal
ISSN (Online): 3006-2071 | ISSN (Print): 3006-2063
Volume 4 • Issue 4 • August 2026

decreases from 1.6901 at (R_d=0) to 1.3450 at (R_d=0.5), 1.1389 at (R_d=1), and 0.8939 at (R_d=2). Thus, an increase in thermal radiation produces a systematic reduction in the conductive component of the wall heat-transfer rate. This behavior is consistent with previous studies of radiative nanofluid and non-Newtonian boundary-layer flows, in which radiation modifies the thermal boundary layer by increasing the effective thermal transport and consequently changing the wall temperature gradient and Nusselt number [21, 22]. It is important to distinguish between the conductive heat-transfer measure reported in Table 3 and the total radiation-inclusive wall heat flux. The values listed in the table correspond to the conductivity-weighted conductive contribution. If the total wall heat flux is evaluated using Eq. (35), the radiation contribution must additionally be included through the factor ((1+R_d)). Therefore, the decrease in the conductive Nusselt measure should not be interpreted as a complete measure of the total energy transported from the wall when thermal radiation is significant.

Overall, the results in Table 3 demonstrate that thermal radiation has a negligible direct influence on the hydrodynamic quantities but a substantial influence on heat transfer. The invariance of (-f''(0)) and (C_fRe_x^{1/2}) confirms the decoupled role of radiation in the momentum equation, whereas the marked reduction in (-\theta'(0)) and the conductive Nusselt measure highlights its importance in controlling thermal transport. These findings agree with the established role of Rosseland radiation in enhancing effective thermal diffusion in radiative boundary-layer and nanofluid systems [22]. The decrease in the wall-temperature gradient with increasing R_d is further illustrated in Figure 3.

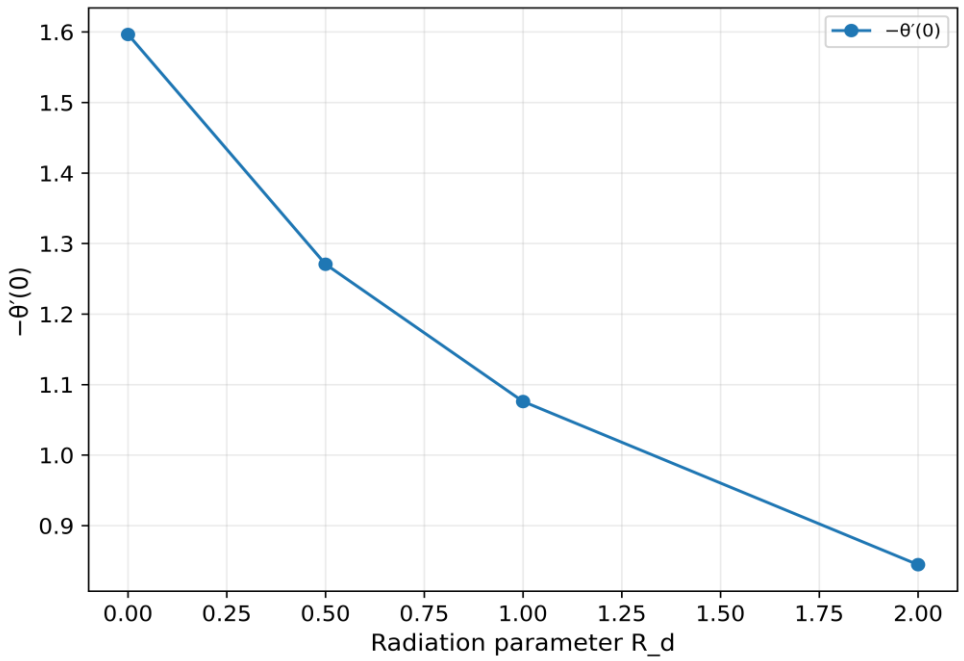


Figure 3. Variation of the dimensionless wall-temperature gradient, −θ′(0), with the radiation parameter R_d.

Table 3. Effect of thermal radiation on flow and heat-transfer characteristics.

R_d	−f″(0)	−θ′(0)	C_f Re_x^1/2	Conductive Nu_x Re_x^−1/2
0.0	0.7098	1.5967	1.4195	1.6901
0.5	0.7098	1.2707	1.4195	1.3450

JOURNAL FOR SOCIAL SCIENCE STUDIES
An International Peer-Reviewed Open Access Journal
ISSN (Online): 3006-2071 | ISSN (Print): 3006-2063
Volume 4 • Issue 4 • August 2026

1.0	0.7098	1.0760	1.4195	1.1389
2.0	0.7098	0.8445	1.4195	0.8939

3.4 Effect of internal heat generation

The internal heat-generation parameter (Q) represents the volumetric production of thermal energy within the fluid. Unlike the Casson parameter and thermal radiation, (Q) appears only in the energy equation in the present formulation and therefore directly modifies the thermal field without producing a direct change in the momentum equation. The numerical results presented in Table 4 clearly demonstrate this separation between the hydrodynamic and thermal responses.As (Q) increases from 0 to 0.4, the wall-temperature gradient (-\theta'(0)) decreases progressively from 1.4026 to 0.7922, as shown in Table 4. This reduction indicates that internal heat generation adds thermal energy to the fluid within the boundary layer, thereby increasing the fluid temperature and reducing the temperature difference between the wall and the adjacent fluid. Consequently, the magnitude of the wall temperature gradient becomes smaller. The corresponding conductivity-weighted heat-transfer measure also decreases substantially from 1.4846 at (Q=0) to 0.8385 at (Q=0.4) (Table 4). This behavior indicates that stronger internal heat generation reduces the amount of heat that must be transferred conductively from the stretching surface to the fluid because a portion of the thermal energy is generated internally.

The intermediate values further confirm this systematic trend. At (Q=0.1), (-\theta'(0)) decreases to 1.2707 and the conductive heat-transfer measure becomes 1.3450. When (Q) is increased to 0.2, these quantities decrease further to 1.1273 and 1.1932, respectively. At the highest investigated value (Q=0.4), the corresponding values reach 0.7922 and 0.8385 (Table 4). Thus, the effect of heat generation becomes increasingly pronounced as the strength of the volumetric energy source increases. Similar reductions in the wall temperature gradient and Nusselt number have been reported for boundary-layer flows with internal heat generation, where the additional thermal energy raises the fluid temperature and weakens the wall-to-fluid temperature gradient [23, 24].

In contrast, the hydrodynamic quantities remain completely unchanged with (Q). As reported in Table 4, (-f''(0)) remains constant at 0.7098 and (C_fRe_x^{1/2}) remains 1.4195 for all values of (Q). This invariance is physically consistent with the present mathematical model because the heat-generation term is included exclusively in the energy equation and does not appear in the reduced momentum equation. Therefore, changes in (Q) alter the thermal boundary layer without directly modifying the velocity boundary layer or wall shear stress. The results in Table 4 demonstrate that internal heat generation is primarily a thermal control parameter in the present Casson nanofluid model. Increasing (Q) strengthens the thermal state of the boundary layer, reduces the wall temperature gradient, and consequently decreases the conductive heat-transfer rate. Meanwhile, the unchanged skin-friction response confirms that the influence of (Q) is confined to the thermal field under the assumptions adopted in the present study. These observations are consistent with previous investigations of heat-generating boundary-layer flows, which have established that volumetric heat sources can substantially modify temperature distributions and surface heat-transfer rates while leaving the momentum solution unchanged when no thermal–momentum coupling term is introduced [25, 26].

JOURNAL FOR SOCIAL SCIENCE STUDIES
An International Peer-Reviewed Open Access Journal
ISSN (Online): 3006-2071 | ISSN (Print): 3006-2063
Volume 4 • Issue 4 • August 2026

Table 4. Effect of internal heat generation on flow and heat-transfer characteristics.

Q	−f″(0)	−θ′(0)	C_f Re_x^1/2	Conductive Nu_x Re_x^−1/2
0.0	0.7098	1.4026	1.4195	1.4846
0.1	0.7098	1.2707	1.4195	1.3450
0.2	0.7098	1.1273	1.4195	1.1932
0.4	0.7098	0.7922	1.4195	0.8385

3.5 Effect of Al_2O_3 nanoparticle volume fraction

The nanoparticle volume fraction (\phi), is an important parameter for controlling the effective thermophysical properties of the Al_2O_3–water nanofluid. Increasing (\phi) modifies the effective density, viscosity, heat capacity, and thermal conductivity of the suspension and consequently influences both momentum and thermal transport. The numerical results for different values of (\phi) are presented in Table 5. Increasing the nanoparticle volume fraction from 0 to 0.04 produces only a small increase in the wall velocity gradient, with (-f''(0)) increasing from 0.7071 to 0.7109. A similar but modest increase is observed in the dimensionless skin-friction coefficient, (C_fRe_x^{1/2}), which rises from 1.4143 at (\phi=0) to 1.4218 at (\phi=0.04). This behavior can be attributed primarily to the increase in effective viscosity associated with nanoparticle addition. The higher particle loading increases the resistance to fluid deformation and consequently produces a slight increase in the wall shear response. Similar weak increases in skin friction with nanoparticle concentration have been reported for nanofluid flow over stretching surfaces, where changes in effective viscosity modify the momentum boundary layer [27].

The thermal response exhibits a more noticeable variation with nanoparticle concentration. According to Table 5, the wall-temperature gradient (-\theta'(0)) decreases progressively from 1.3173 for the pure base fluid ((\phi=0)) to 1.2937, 1.2707, 1.2484, and 1.2266 for (\phi=0.01), 0.02, 0.03, and 0.04, respectively. This gradual reduction indicates that nanoparticle addition alters the thermal boundary-layer structure and increases the effective thermal transport capability of the suspension. The decrease in (-\theta'(0)) reflects the modified dimensionless temperature distribution resulting from the simultaneous changes in the effective thermal properties of the nanofluid. Interestingly, the conductive heat-transfer measure shows the opposite trend. As reported in Table 5, (Nu_xRe_x^{-1/2}) increases from 1.3173 at (\phi=0) to 1.3728 at (\phi=0.04). This increase is consistent with the Maxwell effective thermal-conductivity model used in the present study, according to which incorporating highly conductive Al_2O_3 nanoparticles into water enhances the effective thermal conductivity of the suspension. Consequently, the physical heat-transfer capability can increase even when the dimensionless wall-temperature gradient decreases. This distinction is important when interpreting nanofluid results because the Nusselt number depends not only on the temperature gradient but also on the effective thermal conductivity. Similar enhancement of heat-transfer rates with increasing nanoparticle concentration has been widely reported for Al_2O_3-based nanofluids and other nanoparticle suspensions [28].

The results therefore demonstrate a competition between hydrodynamic and thermal effects. Increasing (\phi) slightly increases the momentum resistance and wall shear, as reflected by the small increase in (-f''(0)) and (C_fRe_x^{1/2}) (Table 5). In contrast, the enhanced effective thermal conductivity associated with Al_2O_3 addition improves the conductive heat-transfer measure. Thus, nanoparticle loading provides a means of enhancing thermal transport, although this benefit is accompanied by a small increase in hydrodynamic resistance. The above results indicate that the influence of Al_2O_3 nanoparticle concentration is relatively modest

JOURNAL FOR SOCIAL SCIENCE STUDIES
An International Peer-Reviewed Open Access Journal
ISSN (Online): 3006-2071 | ISSN (Print): 3006-2063
Volume 4 • Issue 4 • August 2026

on the momentum field but more significant for heat transfer. The decrease in (-\theta'(0)) should not be interpreted independently as a reduction in heat-transfer performance because the effective thermal conductivity simultaneously increases. The resulting increase in the conductive Nusselt measure from 1.3173 to 1.3728 confirms that, within the investigated range, increasing Al_2O_3 concentration enhances the predicted conductive heat-transfer capability of the nanofluid. These findings are consistent with the established role of high-conductivity nanoparticles in improving the thermal performance of water-based nanofluids [29].

Table 5. Effect of Al_2O_3 nanoparticle volume fraction on flow and heat-transfer characteristics.

φ	−f″(0)	−θ′(0)	C_f Re_x^1/2	Conductive Nu_x Re_x^−1/2
0.00	0.7071	1.3173	1.4143	1.3173
0.01	0.7086	1.2937	1.4173	1.3311
0.02	0.7098	1.2707	1.4195	1.3450
0.03	0.7105	1.2484	1.4210	1.3589
0.04	0.7109	1.2266	1.4218	1.3728

3.6 Combined influence of radiation and heat generation

Radiation and internal heat generation influence the thermal field through distinct but interacting mechanisms. Thermal radiation modifies the energy transport process by increasing the effective thermal diffusion through the factor ((1+R_d)). As the radiation parameter (R_d) increases, radiative heat transfer becomes more pronounced, allowing thermal energy to redistribute more efficiently within the fluid. This enhanced thermal transport modifies the temperature distribution and can produce a more gradual variation of temperature across the thermal boundary layer. Similar effects of thermal radiation on temperature distributions and heat-transfer characteristics have been reported in boundary-layer flow studies employing the Rosseland radiation approximation [1,2]. In particular, the inclusion of radiation introduces an additional mode of energy transport that becomes increasingly important under high-temperature conditions [2,3]. In contrast, internal heat generation introduces thermal energy directly into the fluid through the volumetric source term (Q\theta). Therefore, an increase in the heat-generation parameter supplies additional energy throughout the fluid domain and consequently increases the fluid temperature. Unlike radiation, which primarily redistributes thermal energy, internal heat generation acts as a direct source of energy. Previous studies of boundary-layer flows with heat generation or absorption have similarly demonstrated that increasing the heat-generation parameter generally enhances the temperature field and modifies the wall heat-transfer characteristics [4,5]. Recent studies involving non-Newtonian and nanofluid systems have also reported an increase in temperature with increasing heat-generation parameters [6].

When radiation and internal heat generation are simultaneously present, the resulting temperature distribution is governed by the competition between enhanced radiative diffusion and volumetric thermal energy production. At relatively low values of (Q), the effect of radiation can become more apparent because the additional radiative transport facilitates the redistribution of thermal energy within the fluid. However, as (Q) increases, the continuous generation of heat can dominate the thermal response and produce a substantially higher temperature field. Thus, the two parameters should not be regarded as equivalent thermal mechanisms: radiation primarily influences the redistribution and transport of thermal energy, whereas internal heat generation directly increases the energy content of the fluid. This distinction is consistent with earlier numerical investigations

JOURNAL FOR SOCIAL SCIENCE STUDIES
An International Peer-Reviewed Open Access Journal
ISSN (Online): 3006-2071 | ISSN (Print): 3006-2063
Volume 4 • Issue 4 • August 2026

in which radiation and heat-source effects were found to produce significant changes in temperature profiles and heat-transfer rates [4,5]. The combined action of these mechanisms also affects the thermal boundary layer and surface temperature gradient. Internal heat generation tends to increase the thermal energy retained within the fluid and can consequently thicken the thermal boundary layer. Radiation, on the other hand, facilitates thermal redistribution and can alter the rate at which heat is transported away from the heated surface. The interaction between the two effects may therefore produce a nonlinear response in the temperature field and local or average Nusselt number. Studies considering radiation in nanofluid and non-Newtonian flow systems have confirmed that variations in the radiation parameter can significantly modify the temperature field and heat-transfer characteristics [30]. These findings support the present interpretation that the thermal response depends not only on the magnitude of each parameter individually but also on their combined contribution to the energy equation. From a physical and engineering perspective, the simultaneous consideration of radiation and internal heat generation is particularly important in systems operating at elevated temperatures, where radiative transport cannot be neglected and volumetric heat sources may be present. Such conditions can occur in thermal processing, energy-conversion systems, high-temperature manufacturing, electronic thermal management, and chemically reactive transport. Therefore, incorporating both (R_d) and (Q) provides a more realistic representation of the thermal behavior of the system and helps identify operating conditions under which thermal gradients, surface heat transfer, and temperature levels can be effectively controlled.

3.7 Newtonian limiting-case verification

The Newtonian limit is obtained by allowing $\beta \to \infty$. In this limit, $(1 + 1/\beta) \to 1$ and $A_m \to \nu_{nf}/\nu_f$, so the momentum equation becomes

$$f''' + (\nu_f/\nu_{nf})[f f'' - (f')^2] = 0 \quad (41)$$

For the reference calculations, $-f''(0)$ approaches approximately unity as β becomes very large. Recovery of this limiting behavior supports the internal consistency of the Casson correction and similarity transformation used in the numerical formulation. This limiting behavior indicates that the non-Newtonian effects associated with the Casson parameter gradually diminish as (\beta) increases, causing the flow to approach the corresponding Newtonian nanofluid behavior. The convergence of (-f''(0)) toward approximately unity further confirms that the wall-shear response is consistent with the expected Newtonian limit. Similar limiting behavior has been reported in previous studies of Casson-fluid boundary-layer flows [31, 32, 33]. Thus, the present result provides an important validation of the governing momentum equation and the numerical formulation

3.8 Physical and engineering interpretation

The numerical findings indicate that rheological and thermal controls should be interpreted separately but collectively. The Casson parameter primarily controls the momentum field and wall shear, while radiation and internal heating act directly on the energy equation. Nanoparticle loading affects both thermal conductivity and other effective properties, so optimization cannot be based on conductivity alone. In polymer extrusion and coating processes, the coupled velocity and temperature boundary layers influence cooling, viscosity, solidification, and final surface quality. In high-temperature thermal management, radiation can strongly alter the thermal response without directly changing the hydrodynamic solution under the present assumptions.

These results emphasize the strongly coupled nature of transport phenomena in practical non-Newtonian nanofluid systems. Changes in rheological properties can modify the flow resistance and wall shear, whereas thermal parameters primarily regulate temperature distribution and heat-transfer performance. The combined effects are therefore important when selecting operating conditions for industrial processes. In extrusion and coating applications, appropriate control of rheology,

ISSN (Online): 3006-2071 | ISSN (Print): 3006-2063
Volume 4 • Issue 4 • August 2026

nanoparticle concentration, and thermal conditions can help maintain uniform cooling and improve product quality. Similarly, in high-temperature applications, incorporating thermal radiation is essential for accurate prediction of the thermal field and overall heat-transfer behavior.

4. Conclusion

A numerical study of steady Casson Al_2O_3–water nanofluid flow over a linearly stretching sheet was conducted by incorporating thermal radiation and uniform internal heat generation. The results demonstrate that the Casson parameter is the dominant control on wall-shear behavior, with the dimensionless skin-friction response decreasing from 1.7388 at a Casson parameter of 0.5 to 1.0527 at 10 and approaching the Newtonian limiting value of approximately unity. Thermal radiation has a pronounced effect on the thermal field, with an increase in the radiation parameter from 0 to 2 reducing the wall-temperature gradient from 1.5967 to 0.8445. Internal heat generation increases the thermal energy of the boundary layer and consequently decreases the wall-temperature gradient and conductive heat-transfer response, while the velocity field remains essentially unaffected. Increasing the Al_2O_3 volume fraction from 0 to 0.04 also reduces the wall-temperature gradient but increases the conductivity-weighted heat-transfer measure from 1.3173 to 1.3728 because of the enhanced effective thermal conductivity. For the reference condition of Casson parameter 1, nanoparticle volume fraction 0.02, radiation parameter 0.5, and heat-generation parameter 0.1, the dimensionless skin-friction response is approximately 1.4195, the wall-temperature gradient is 1.2707, and the conductive heat-transfer measure is approximately 1.3450. The recovery of the Newtonian limiting behavior provides additional verification of the mathematical formulation and numerical solution. Overall, the study confirms that Casson rheology, nanoparticle concentration, thermal radiation, and internal heat generation jointly control the thermal and flow characteristics and should therefore be considered simultaneously in practical non-Newtonian nanofluid heat-transfer applications.

5. Limitations of the Study

The present study has several limitations. The Al_2O_3–water nanofluid is modeled using a single-phase effective-property approach, without explicitly considering Brownian diffusion and thermophoresis, while thermophysical properties are assumed constant except for their dependence on nanoparticle volume fraction. The Rosseland radiation model applies mainly to optically thick media, and viscous dissipation is neglected. In addition, magnetic effects, porous-medium resistance, chemical reactions, slip, suction/injection, and convective boundary conditions are not considered. The analysis is restricted to steady, two-dimensional flow over a linearly stretching sheet, excluding transient, three-dimensional, and nonlinear stretching effects. Experimental validation and a separate systematic grid-independence or benchmark comparison are also not included; therefore, model verification relies mainly on numerical convergence and recovery of the Newtonian limiting behavior.

Declarations

Ethical Approval

The collection of plant material must comply with relevant institutional, national, and international guidelines and legislation. Our study complies with relevant institutional, national, and international guidelines and legislation.

Consent to Participate

Not applicable.

Consent to Publish

Not applicable.

Author declaration

All authors agree to publish the work in its current form.

Clinical Trial Number

Not applicable

ISSN (Online): 3006-2071 | ISSN (Print): 3006-2063
Volume 4 • Issue 4 • August 2026

Author Contributions

Abdul Razaq: Conceptualization, methodology, investigation, data collection, formal analysis, and writing—original draft. Shawal Rizwan: Conceptualization, supervision, methodology, validation, project administration, and writing—review and editing. Zahid Nawaz: Investigation, data curation, formal analysis, and writing—original draft. Hamza Khan: Methodology, investigation, data analysis, visualization, and writing—review and editing. Kiramat Ullah and Rabail Urooj: Validation, visualization, literature review, and writing—review and editing. All authors read and approved the final version of the manuscript.

Funding: Not applicable

Competing Interest

The authors declare that they have no competing interests.

Availability of Data and Materials

All relevant data generated or analyzed during this study are included in this manuscript. Additional data may be made available upon reasonable request from the corresponding authors.

Acknowledgments

We are thankful to all the authors who participated in this research work.

References

Das, S. K., Choi, S. U., & Patel, H. E. (2006). Heat transfer in nanofluids—a review. Heat transfer engineering, 27(10), 3-19.

Goudarzi, S., Shekaramiz, M., Omidvar, A., Golab, E., Karimipour, A., & Karimipour, A. (2020). Nanoparticles migration due to thermophoresis and Brownian motion and its impact on Ag-MgO/Water hybrid nanofluid natural convection. Powder Technology, 375, 493-503.

Chhabra, R. P., & Patel, S. A. (2023). Bubbles, drops, and particles in non-Newtonian fluids. CRC press.

Kausar, M. S., Ali, A. B., Anwar, T., Nasir, M., Saleem, S., Waqas, M., & Walelign, T. (2025). Thermal energy optimization in Darcy-Forchheimer slip flow featuring viscoplastic (Casson) model subjected to diffusion of chemically reactive species. Case Studies in Thermal Engineering, 107359.

Mandal, G., Kaswan, P., Sarkar, A., & Kezzar, M. (2026). Enhanced heat transfer characteristics of Casson–Williamson trihybrid nanofluid under quadratic thermal radiation over a porous stretching surface. International Journal of Numerical Methods for Heat & Fluid Flow, 36(8), 3273-3307.

Islam, M. R., Hossain, A., Biswas, R., Hasan, M., Rana, B. J., Habibullah, H., & Afikuzzaman, M. (2025). Modelling and theoretical overview of Casson fluid flow through a stretching sheet with variable viscosity and sinusoidal boundary conditions. International Journal of Ambient Energy, 46(1), 2539139.

Khan, I., & Ahmed Khan, M. W. (2024). Artificial neural networking for computational assessment of ternary hybrid nanofluid flow caused by a stretching sheet: implications of machine-learning approach. Engineering Applications of Computational Fluid Mechanics, 18(1), 2411786.

Damm, D. L., & Fedorov, A. G. (2005). Radiation heat transfer in SOFC materials and components. Journal of Power Sources, 143(1-2), 158-165.

Ghadikolaei, S. S., Hosseinzadeh, K., Ganji, D. D., & Jafari, B. (2018). Nonlinear thermal radiation effect on magneto Casson nanofluid flow with Joule heating effect over an inclined porous stretching sheet. Case studies in thermal engineering, 12, 176-187.

Alali, E., & Megahed, A. M. (2022). MHD dissipative Casson nanofluid liquid film flow due to an unsteady stretching sheet with radiation influence and slip velocity phenomenon. Nanotechnology Reviews, 11(1), 463-472.

ISSN (Online): 3006-2071 | ISSN (Print): 3006-2063
Volume 4 • Issue 4 • August 2026

Afridi, M. I., & Qasim, M. (2018). Entropy generation and heat transfer in boundary layer flow over a thin needle moving in a parallel stream in the presence of nonlinear Rosseland radiation. International Journal of Thermal Sciences, 123, 117-128.

Cakmak, Y. O., Ayli, E., & Yapici, E. Ö. (2026). Thermo-hydraulic performance evaluation of hybrid nanofluids with twisted tape inserts using a PEC-based approach. Journal of Mechanical Science and Technology, 1-14.

Alatawi, A., Alshaban, E., Aldhabani, M. S., & Alrihieli, H. (2025). Dynamic-behavior of Casson-type hybrid nanofluids due to a stretching sheet under the coupled impacts of boundary slip and reaction-diffusion processes. Nanotechnology Reviews, 14(1), 20250244.

Shuaib, M., Anas, M., Rehman, H. U., Khan, A., Khan, I., & Eldin, S. M. (2023). Volumetric thermo-convective casson fluid flow over a nonlinear inclined extended surface. Scientific Reports, 13(1), 6324.

Nasir, M., Kausar, M. S., Waqas, M., Beg, O. A., & Khan, W. A. (2025). Computational analysis of magnetized Casson liquid stretching flow adjacent to a porous medium with Joule heating, stratification, multiple slip and chemical reaction aspects. Numerical Heat Transfer, Part A: Applications, 86(13), 4464-4486.

Venkatesh, N., Kumar, M. A., Reddy, Y. D., Raju, R. S., & Pothanna, N. (2026). Thermal and electromagnetic transport in Casson fluid flow through porous media with radiation and heat source effects: a numerical study. Journal of Thermal Analysis and Calorimetry, 1-15.

Mandal, G., Kaswan, P., Sarkar, A., & Kezzar, M. (2026). Enhanced heat transfer characteristics of Casson–Williamson trihybrid nanofluid under quadratic thermal radiation over a porous stretching surface. International Journal of Numerical Methods for Heat & Fluid Flow, 36(8), 3273-3307.

Ilango, M. S., & Lakshminarayana, P. (2024). Effects of double diffusion and induced magnetic field on convective flow of a Casson nanofluid over a stretching surface. Heliyon, 10(10).

Bakar, M. M. A., Ullah, A., Khan, A., Hussain, S. M., Eid, M. R., & Guedri, K. (2026). Heat Transfer Characteristics of Radiative Sodium Alginate–MoS2 Burgers Nanofluid over a Stretching Surface with Convective Heating. Results in Surfaces and Interfaces, 100902.

Abdullah, Pan, K., Shah, N. A., Khan, N. M., & Shakeel, M. (2026). Modeling hybrid nanoparticle transport in a non-Newtonian MHD flow over parabolic surfaces: influence of thermal radiation and Brownian motion. Multidiscipline Modeling in Materials and Structures, 22(4), 942-961.

Hossain, M. R. (2022). Effect of thermal radiation on MHD mixed convection in an encloser with semicircular heater using kerosene based CNT nanofluid.

Gubena, T., & Ibrahim, W. (2026). Thermal Radiative Flow and Entropy Generation in MHD Williamson Hybrid Nanofluid (Cu+ Ag)/H2O Over a Porous Stretching Sheet With Non-Fourier Heat Flux and Heat Source. Advances in Mathematical Physics, 2026(1), 4016593.

Venu, T., Shamshuddin, M. D., & Salawu, S. O. (2026). Buoyancy-Driven Micropolar Fluid Flow Transport in Porous Media With Variable Heat Source and Convective Heating. Asia-Pacific Journal of Chemical Engineering, 21(1), e70130.

Swain, B. K., Sahoo, C. S., & Dash, G. C. (2026). Impact of Non-linear Boussinesq approximation on unsteady MHD free convective flow through porous medium: a numerical and ANN-Based analysis. Thermal Advances, 100185.

ISSN (Online): 3006-2071 | ISSN (Print): 3006-2063
Volume 4 • Issue 4 • August 2026

Alrehili, M. (2023). Improvement for engineering applications through a dissipative Carreau nanofluid fluid flow due to a nonlinearly stretching sheet with thermal radiation. Case Studies in Thermal Engineering, 42, 102768.

Minh, C. N. (2025). Heat Transfer Enhancement Using Al_2O_3, CuO, and Hybrid Al_2O_3–CuO Nanofluids in Water and Ethylene Glycol–Water Mixtures in an Automotive Radiator. International Journal of Heat & Technology, 43(4), 1429.

Rashid, F. L., Al Maimuri, N. M., Hammoodi, K. A., Eleiwi, M. A., Omle, I., Alsayyad, A. M. M., ... & Hamida, M. B. B. (2025). Application of nanofluids for performance improvement of plate heat exchangers: A comprehensive review. IScience.

Liu, M., Lin, M. C., & Wang, C. (2011). Enhancements of thermal conductivities with Cu, CuO, and carbon nanotube nanofluids and application of MWNT/water nanofluid on a water chiller system. Nanoscale research letters, 6(1), 297.

Kotike, J., Beedalannagari, O., Rekapalli, L., Usman, M., & Kadavakollu, K. R. (2025). Neural network modeling of CuO/Au hybrid nanofluid thermal performance with slip effects for advanced process applications. Processes, 13(2), 516.

Jarwal, V. K., Choudhary, S., Sharma, K., & Choudhary, P. (2025). Modeling and analysis of entropy in MHD unsteady flow of water-based nanofluids with carbon nanoparticles. Discover Applied Sciences, 7(7), 686.

Bilal, S., Malik, M. Y., Hussain, A., & Khan, M. (2017). Effects of temperature dependent conductivity and absorptive/generative heat transfer on MHD three dimensional flow of Williamson fluid due to bidirectional non-linear stretching surface. Results in Physics, 7, 204-212.

Reddy, P. S., & Sreedevi, P. (2024). Enhanced entropy generation and heat transfer characteristics of magnetic nano-encapsulated phase change materials in latent heat thermal energy storage systems. Applied Mathematics and Mechanics, 45(6), 1051-1070.

Hussanan, A., Zuki Salleh, M., Tahar, R. M., & Khan, I. (2014). Unsteady boundary layer flow and heat transfer of a Casson fluid past an oscillating vertical plate with Newtonian heating. PloS one, 9(10), e108763.